DOI: 10.1002/cctc.201100408

Mesoporous Nitrogen Doped Carbon Supported Platinum PEM Fuel Cell Electrocatalyst Made From Ionic Liquids

Frédéric Hasché,*[a] Tim-Patrick Fellinger,[b] Mehtap Oezaslan,[a] Jens Peter Paraknowitsch,[c] Markus Antonietti,[b] and Peter Strasser[a]

A multitude of new and improved catalyst materials and concepts for membrane fuel cells were developed over the last decade. The requirements of these catalysts are low cost, high activity and durability. For example, platinum based catalyst concepts such as Pt monolayer catalysts,[1,2] Pt skin catalysts,[3–5] Pt multimetallic catalysts,[6] and dealloyed bimetallic Pt core-shell nanoparticle catalysts[7–14] show promising activities based on Pt mass and Pt surface area for the oxygen reduction reaction (ORR). Furthermore, non-noble metal catalyst concepts[15–20] could reduce the costs, but they currently still do not meet the activity targets[21] for commercial fuel cell electrocatalysts. To improve the durability of fuel cell catalysts, also the support material is becoming more important. Oxidation resistance of the support material is one point of concern.[22] Alternatives to pure carbon blacks (e.g. Vulcan XC 72R) were evaluated for the oxygen reduction, such as carbon nanotubes,[23,24] silicon carbide derived carbons,[25] hollow spherical carbons,[26] nitrogen modified carbons,[27] or titanium-based materials.[28–30] Especially nitrogen doped carbons show interesting properties like high conductivity,[31] mesoporosity[32] and the opportunity to adjust the nitrogen content[33] in the support material.

In this communication, we report the synthesis of a mesoporous nitrogen doped carbon supported platinum catalyst (Pt/*meso*-BMP) based on an ionic liquid as nitrogen/carbon precursor and the evaluation of the catalytic system for ORR. Further, we analyzed the long-term behavior of this new catalyst and compared it with commercial high surface area carbon (HSAC) supported platinum catalyst.

The mesoporous nitrogen doped carbon supported platinum nanoparticle fuel cell electrocatalyst (Pt/*meso*-BMP) was prepared by a two-step synthesis, as shown in Figure 1. In the first step, the mesoporous nitrogen doped carbon material (*meso*-BMP) was synthesized corresponding to the reference[34,35] by using *N*-butyl-3-methylpyridinedicyanamide (BMP-dca) as ionic liquid compound. As evaluated by X-ray photoelectron spectroscopy (XPS) and elemental analysis (EA) the nitrogen content of 14.2 wt.% (XPS)/17.2 wt.% (EA) is very high. The variation of the values can be explained by the surface specificity of XPS measurements. In the second step, platinum nanoparticles were deposited on the *meso*-BMP substrate. The deposition of Pt occurred by a wet impregnation–freeze-drying method and followed by thermal annealing in a reductive atmosphere.[36–38]

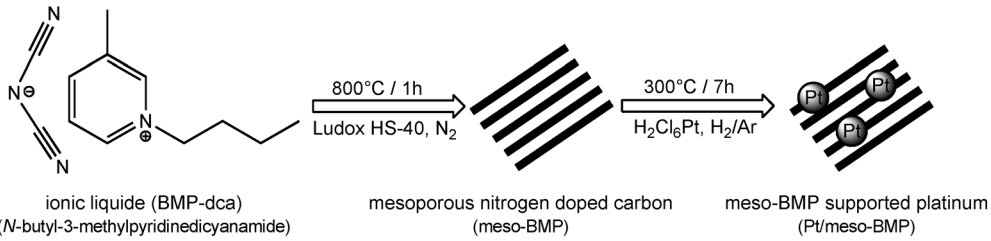

Figure 1. Synthesis route for mesoporous nitrogen doped carbon supported platinum nanoparticle catalyst.

Shown in Figure 2 are the XRD profiles for *meso*-BMP and Pt/*meso*-BMP. The as synthesized *meso*-BMP support material exhibits broad XRD reflections at $2\theta = 26.1$ and 42.9° corresponding to the inter (002) and intra (101) lattice planes of graphitized carbon. The reference powder diffraction patterns of (111), (200), and (220) lattice planes for pure face centered

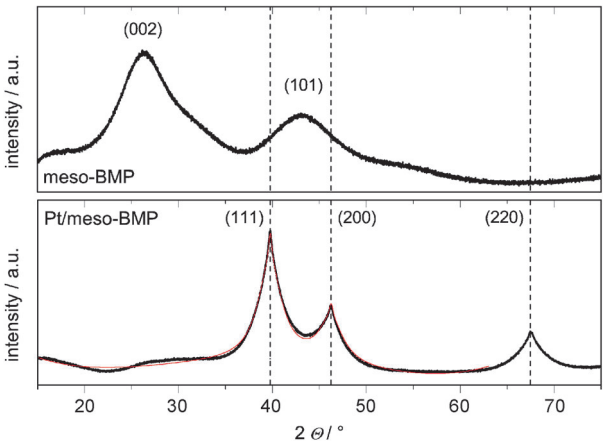

Figure 2. XRD profiles of the *meso*-BMP support material (top) and Pt/*meso*-BMP catalyst (bottom) with a Rietveld refinement fit (thin red line). Vertical dotted lines denote reference powder diffraction patterns of pure fcc Pt, PDF(Pt)#00-004-0802.[39]

[a] *F. Hasché, M. Oezaslan, Prof. Dr. P. Strasser*
The Electrochemical Energy, Catalysis, and Materials Science Laboratory
Institut für Chemie,
Technische Universität Berlin, 10623 Berlin (Germany)
Fax: (+49) 30-314-22261
E-mail: frederic.hasche@tu-berlin.de

[b] *T.-P. Fellinger, Prof. Dr. M. Antonietti*
Department of Colloid Chemistry
Max Planck Institute of Colloids and Interfaces
Research Campus Golm, 14424 Potsdam (Germany)

[c] *Dr. J. P. Paraknowitsch*
Functional Materials
Institut für Chemie
Technische Universität Berlin, 10623 Berlin (Germany)

cubic (fcc) Pt[39] are indicated with the vertical dotted lines. The asymmetric shape of the XRD reflections for pure fcc Pt signifies different crystallite sizes. According to the Rietveld analysis, Pt nanoparticles show a mean crystallite size of 1.9 ± 0.1 nm as the main crystal phase of 95.9 ± 1.5 wt.%, while the minor crystal phase (4.1 ± 1.5 wt.%) exhibits a mean crystallite size of 15.2 ± 3.0 nm. This size result conforms excellently to the mean particle size of 2.3 ± 0.6 nm established by transmission electron microscopy (TEM).

Shown in Figure 3 are the TEM images of the as synthesized Pt/*meso*-BMP. Here, the established mesoporosity of the nitrogen doped carbon supported Pt material is visible (Figure 3a), as well as the good dispersion of Pt nanoparticles on the support material (Figure 3b).

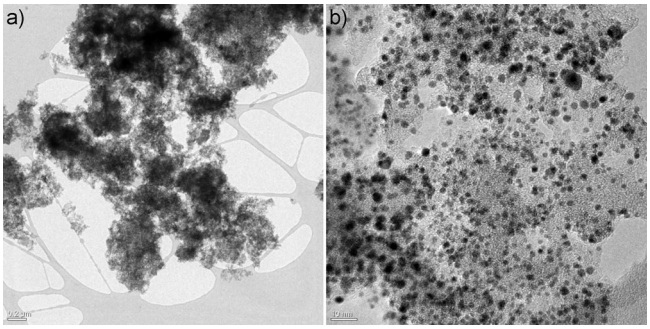

Figure 3. TEM images for the as synthesized Pt/*meso*-BMP: a) 0.2 μm scale bar, b) 10 nm scale bar.

In the following, we tested the as synthesized Pt/*meso*-BMP nanoparticle catalyst for the electroreduction of dioxygen to water to compare its activity with a benchmark commercial HSAC supported pure Pt nanoparticle catalyst. Shown in Figure 4a are the polarization curves for Pt/*meso*-BMP at various rotation speeds in oxygenated 0.1 M $HClO_4$ at room temperature established by rotating disc electrode (RDE) technique to construct a Koutecky–Levich plot, as shown in Figure 4b. All

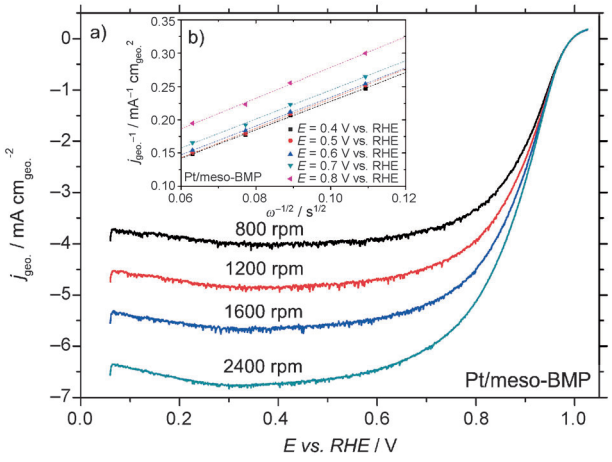

Figure 4. Electrochemical characterization of Pt/*meso*-BMP, a) polarization curves at various rotation speeds in oxygenated 0.1 M $HClO_4$, b) Koutecky–Levich plot for oxygen reduction at various voltages.

polarization curves exhibited a plateau behavior between 0.06–0.60 V versus RHE, indicating the diffusion controlled regime. The current density increases with increasing rotation speed. Thereby, the oxygen diffusion to the catalytic reaction center is the rate limiting process and in consequence dependent on the rotation rate.[40,41] The diffusion controlled regime turns into a mixed diffusion–kinetic controlled regime at higher voltages. Finally, from about 0.85 V versus RHE, the reaction rate is only kinetically controlled, as judged by the independence of the rotation rate. At the open circuit potential (around 1.0 V versus RHE), eventually no electrocatalytic conversion of oxygen was observed.

The selectivity of Pt/*meso*-BMP for the direct oxygen reduction was established from the Koutecky–Levich plot; the experimental values of Figure 4a were replotted in Figure 4b using the following relationship in Equation (1):

$$\frac{1}{j} = \frac{1}{j_{kinetic}} + \frac{1}{j_{diffusion}} = \frac{1}{j_{kinetic}} + \frac{1}{(B \cdot \omega^{1/2})} \qquad (1)$$

$$B = 0.62\, n \cdot F \cdot D(O_2)^{2/3} \cdot \nu^{-1/6} \cdot c(O_2)$$

For which j, $j_{kinetic}$, and $j_{diffusion}$ are the current density, kinetic current density, and diffusion limiting current density, respectively, and ω is the rotation rate. The number of electrons transferred per oxygen molecule can be determined from the Koutecky–Levich slope (B). The so called "B Factor" is dependent on the experimental conditions and allows a comparison with the theoretical value for an ideal direct four electron process of oxygen reduction [Eq. (2)]. Published data were used for the oxygen solubility ($c(O_2)$), the diffusivity ($D(O_2)$), the Faraday constant (F) and the kinematic viscosity of the electrolyte (ν).[42]

$$O_2 + 4\,H^+ + 4\,e^- \rightarrow 2\,H_2O \qquad (2)$$

The experimental "B Factor" was calculated and averaged at various voltages from the slop of the Koutecky–Levich Plot (Figure 4b) and is 0.454 ± 0.012 mA $cm_{geo}^{-2}\, s^{1/2}$. This value is in excellent agreement with the theoretical "B Factor" for a direct four electron process (0.467 mA $cm_{geo}^{-2}\, s^{1/2}$, deviation $< 3\%$).

Summarized in Table 1 are the as synthesized mean particle size values, Pt mass based (j_{mass}) and Pt surface area specific based ($j_{specific}$) activities of Pt/*meso*-BMP for ORR compared with commercial benchmark pure Pt/HSAC. The Pt/*meso*-BMP shows similar j_{mass} compared with the Pt/HSAC by similar particle size and is in good agreement with published values.[23,43,44] With

Table 1. Comparison of as synthesized mean particle size, Pt mass and Pt surface area specific based ORR activities for Pt/*meso*-BMP and Pt/HSAC nanoparticle catalysts.

Catalyst	Mean particle size [nm]	ECSA [$m^2\, g_{Pt}^{-1}$]	j_{mass} [A mg_{Pt}^{-1}][a]	$j_{specific}$ [μA cm_{Pt}^{-2}][a]
Pt/*meso*-BMP	2.3 ± 0.6	98 ± 9	0.12 ± 0.03	127 ± 20
Pt/HSAC	2.3 ± 0.7	74 ± 7	0.14 ± 0.01	191 ± 20

[a] 0.9 V versus RHE.

a view to the Pt electrochemically active surface area (ECSA), the Pt/*meso*-BMP exhibits clearly higher ECSA than the Pt/HSAC.

To evaluate whether this ECSA benefit translates in improved stability characteristics, a voltage cycling long-term stability test was performed for Pt/*meso*-BMP and Pt/HSAC nanoparticle catalysts. The catalysts were subjected to 10000 voltage cycles between 0.5–1.0 V versus RHE with a scan rate of 50 mV s^{-1} in deaerated 0.1 M $HClO_4$ at room temperature. Such a voltage cycling protocol is an accelerated degradation test to assess the long-term behavior of fuel cell electrocatalysts.[11,12,23] Shown in Figure 5 are the resulting absolute ECSA trends (inset, normalized ECSA trend) for Pt/*meso*-BMP and Pt/HSAC during the voltage cycling.

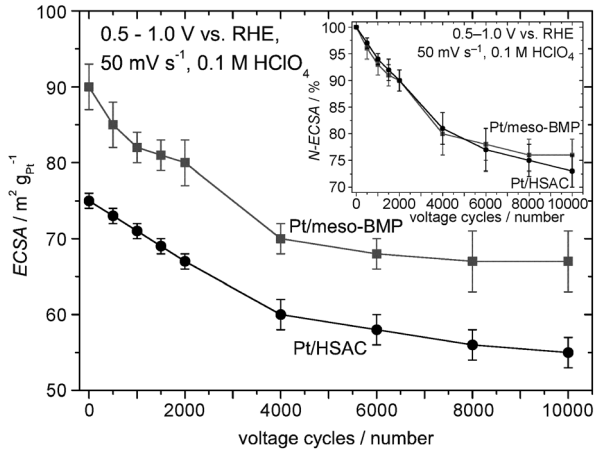

Figure 5. Evolution of the platinum electrochemical active surface area (ECSA) (inset: normalized ECSA trend) for Pt/*meso*-BMP (red squares) and Pt/HSAC (black circles) during voltage cycling from 0.5 to 1.0 V versus RHE with 50 mV s^{-1} in deaerated 0.1 M $HClO_4$ electrolyte at room temperature.

The ECSA values for Pt/*meso*-BMP nanoparticle catalyst are clearly higher than those for Pt/HSAC before and after voltage cycling testing. In results, the ECSA decreased from 90 ± 3 $m^2 g_{Pt}^{-1}$ to 67 ± 4 $m^2 g_{Pt}^{-1}$ (−26%) and 75 ± 1 $m^2 g_{Pt}^{-1}$ to 55 ± 2 $m^2 g_{Pt}^{-1}$ (−27%) for Pt/*meso*-BMP and Pt/HSAC, respectively. The ECSA loss is associated with mean particle size growth for Pt/*meso*-BMP (2.3 ± 0.6 nm to 3.3 ± 0.9 nm) and Pt/HSAC (2.3 ± 0.7 nm to 3.1 ± 0.7 nm) and carbon corrosion. It is noted, that the normalized ECSA loss and curve trend are very similar for both Pt catalysts and indicate an equal behavior of degradation for both catalysts (see Figure 5 inset). This corresponds to earlier studies with different carbon supported Pt and Pt alloy nanoparticles, where the ECSA loss curve can be split into two regimes.[11,12,23] We observed that in the earlier stage (up to 4000 voltage cycles) particle growth controls primarily the degradation mechanism while in the later stage carbon (support) corrosion associated with particle detachment is dominant.

In conclusion, we have synthesized a novel catalyst type of mesoporous nitrogen doped carbon supported platinum catalyst for the electrocatalytic reduction of oxygen. The new catalyst shows comparable activities like the benchmark commercial fuel cell Pt catalyst. A significantly increased Pt electrochemical active surface area was established compared to the benchmark catalyst. Further studies are necessary to evaluate and optimize this class of support material which shows promising opportunities for enhanced durability electrocatalysts for fuel cells.

Experimental Section

Synthesis of Pt/meso-BMP

2 g of the ionic liquid N-butyl-3-methylpyridinedicyanamide (BMP-dca, Ionic liquid Technologie GmbH) were mixed with 5 g Ludox HS-40 solution (40 wt.%, aqueous dispersion of SiO_2 nanoparticles, Aldrich, #420816) and carbonized at 800 °C with a heating rate of 10 K min^{-1} and subsequently an isothermal period at 800 °C for 1 hour in nitrogen. The resulted black powder was triturated in a mortar and the SiO_2 template was removed with 4 M NH_4HF_2 solution (40 mL per gram). After washing with water and drying, the black, fine mesoporous nitrogen doped carbon powder (*meso*-BMP) was then wet impregnated with a H_2PtCl_6 hexachloroplatinic acid precursor solution (20 wt.% Pt, Alfa Aesar, #040177). The impregnated powder was freeze dried under vacuum. The dried powder was annealed by 250 °C for 2 h and subsequently 300 °C for 7 h in a tube furnace under reductive atmosphere (4 Vol.% H_2, 96 Vol.% Ar, quality of 5.0, AirLiquide). The Pt/*meso*-BMP catalyst exhibited a calculated Pt loading of 21.4 wt.%. A benchmark, commercial high surface area carbon (HSAC) supported Pt nanoparticle catalyst (28.2 wt.% Pt, TEC10E30E, Lot#108–0331, TKK) was taken for the comparison of ORR activities and ECSA. All chemicals were used as received from the delivery companies.

Structural characterization

The structural characterization of *meso*-BMP and Pt/*meso*-BMP was carried out using powder X-ray diffraction (D8 Advanced, Bruker AXS) with a CuK_α source (40 kV/40 mA) and a position sensitive LynxEye detector (PSD). The following XRD scan parameters were used: 2θ: 15 to 80°, step size: 0.01°, holding time per step: 7 second, variable divergence slit: 4 mm, PSD Iris antiscattering slit: 13, and sample rotation: 15 rpm (rounds per minute). The crystal phase Rietveld quantification and crystallite size were established with TOPAS (Bruker AXS, Version 4–2) using the integral breath method.[45] Furthermore, the particle size distribution and morphology of the Pt catalysts were investigated before and after the long-term voltage cycling test by using transmission electron microscopy (FEI TECNAI G^2 20 S-TWIN) operated by an accelerating voltage of 200 kV. The mean particle size was determined from the TEM images by counting of more than 400 particles (analySIS FIVE software, Soft Imaging Systems, Olympus).

Electrochemical characterization

All electrochemical measurements were performed in a three compartment electrochemical glass cell with 0.1 M $HClO_4$ electrolyte solution (prepared by diluting from a 70% stock solution, Sigma–Aldrich, #311421) at room temperature using a rotating disk electrode (RDE) technique.[46–48] For the RDE experiments a Pt mesh as counter electrode, a mercury-mercury sulfate electrode as reference electrode, a commercial glassy carbon electrode (GC electrode, diameter of 5 mm, PINE Instruments, USA) as working electrode, a commercial potentiostat (VSP-5, BioLogic, France) and

a PINE rotator were used. To prepare a GC electrode with the catalytic thin film, around 5 mg of catalyst powder was suspended via horn sonification in a solution of de-ionized water, 2-propanol and Nafion (5 wt.% of stock solution). 10 μL of this suspension was pipetted onto the previously polished and cleaned GC electrode and dried at 60 °C for 10 min in air. The GC electrode obtained a calculated Pt loading between 12 and 25 $\mu g_{Pt}\,cm_{geo}^{-2}$. The influence of the different Pt mass loadings on the electrochemical performance in this given range is negligible. The polarization curves for the oxygen reduction reaction (ORR) were recorded with a rotating speed of 1600 rpm (rounds per minute) and a scan rate of 5 $mV\,s^{-1}$ in oxygenated 0.1 M $HClO_4$ electrolyte under oxygen atmosphere, by anodic sweeping the voltage from 0.06 V vs. RHE to the open circuit potential (around 1.1 V vs. RHE). The intrinsic kinetic current at 0.9 V vs. RHE was corrected with the mass transport diffusion limiting current between 0.2 and 0.5 V vs. RHE. To establish the platinum electrochemical active surface area (ECSA), cyclic voltammetry (CV) profiles were recorded between 0.06 and 1.00 V vs. RHE with a scan rate of 100 $mV\,s^{-1}$ in deaerated 0.1 M $HClO_4$ electrolyte under nitrogen atmosphere. The ECSA was calculated using the mean integral charge of the hydrogen adsorption/desorption regime with double layer current corrected at 0.4 V vs. RHE and with 210 $\mu C\,cm_{Pt}^{-2}$, assuming one hydrogen atom observed to one platinum atom. The normalized ECSA was calculated as follows: N-ECSA(cycle#) = ECSA(cycle#)/ECSA(initial)*100%. The long-term stability test was performed with 10000 voltage cycles from 0.5 to 1.0 V vs. RHE at a scan rate of 50 $mV\,s^{-1}$ in deaerated 0.1 M $HClO_4$ electrolyte under nitrogen atmosphere. During the run-time, three complete CV profiles (0.06–1.00 V vs. RHE, 100 $mV\,s^{-1}$) were recorded to determine the ECSA. Before the electrochemical characterization of initial ORR activity and the voltage cycling stability started, the catalyst had been voltammetric pretreated with three full CV profiles (0.06–1.00 V vs. RHE, 100 $mV\,s^{-1}$), followed by 200 fast CV profiles (0.06–1.00 V vs. RHE, 500 $mV\,s^{-1}$) and finally three full CV profiles (0.06–1.00 V vs. RHE, 100 $mV\,s^{-1}$). All electrode potentials were converted into and are reported in the reversible hydrogen electrode (RHE) scale. For all reported values of each catalyst, we used data points from five (initial activities) or two (voltage cycling test) independent measurements.

Acknowledgements

The authors especially thank Dipl.-Ing. (F.H.) Sören Selve from Zentraleinrichtung Elektronenmikroskopie at Technische Universität Berlin and Annette Wittebrock. This project was supported by the Technische Universität Berlin, Germany, the Cluster of Excellence in Catalysis (UNICAT) and the Max Planck Society, Germany.

Keywords: fuel cell · ionic liquid · mesoporous materials · nitrogen doped carbon · stability

[1] J. Zhang, Y. Mo, M. B. Vukmirovic, R. Klie, K. Sasaki, R. R. Adzic, *J. Phys. Chem. B* **2004**, *108*, 10955 – 10964.
[2] K. Sasaki, H. Naohara, Y. Cai, Y. M. Choi, P. Liu, M. B. Vukmirovic, J. X. Wang, R. R. Adzic, *Angew. Chem.* **2010**, *122*, 8784 – 8789; *Angew. Chem. Int. Ed.* **2010**, *49*, 8602 – 8607.
[3] V. R. Stamenkovic, B. S. Mun, K. J. J. Mayrhofer, P. N. Ross, N. M. Markovic, *J. Am. Chem. Soc.* **2006**, *128*, 8813 – 8819.
[4] V. Stamenkovic, T. J. Schmidt, P. N. Ross, N. M. Markovic, *J. Phys. Chem. B* **2002**, *106*, 11970 – 11979.
[5] T. Toda, H. Igarashi, H. Uchida, M. Watanabe, *J. Electrochem. Soc.* **1999**, *146*, 3750 – 3756.
[6] C. Wang, D. van der Vliet, K. L. More, N. J. Zaluzec, S. Peng, S. Sun, H. Daimon, G. Wang, J. Greeley, J. Pearson, A. P. Paulikas, G. Karapetrov, D. Strmcnik, N. M. Markovic, V. R. Stamenkovic, *Nano Lett.* **2011**, *11*, 919 – 926.
[7] H. A. Gasteiger, N. M. Markovic, *Science* **2009**, *324*, 48 – 49.
[8] P. Strasser, *Rev. Chem. Eng.* **2009**, *25*, 255.
[9] P. Strasser, S. Koh, T. Anniyev, J. Greeley, K. More, C. Yu, Z. Liu, S. Kaya, D. Nordlund, H. Ogasawara, M. F. Toney, A. Nilsson, *Nat. Chem.* **2010**, *2*, 454 – 460.
[10] M. Oezaslan, F. Hasché, P. Strasser, *Chem. Mater.* **2011**, *23*, 2159 – 2165.
[11] F. Hasché, M. Oezaslan, P. Strasser, *ChemCatChem* **2011**, *3*, 1805 – 1813.
[12] F. Hasché, M. Oezaslan, P. Strasser, *J. Electrochem. Soc.* **2012**, *159*, B25-B34.
[13] M. Oezaslan, P. Strasser, *J. Power Sources* **2011**, *196*, 5240 – 5249.
[14] M. Oezaslan, M. Heggen, P. Strasser, *J. Am. Chem. Soc.* **2012**, *134*, 514 – 524.
[15] F. Jaouen, J. Herranz, M. Lefevre, J.-P. Dodelet, U. I. Kramm, I. Herrmann, P. Bogdanoff, J. Maruyama, T. Nagaoka, A. Garsuch, J. R. Dahn, T. Olson, S. Pylypenko, P. Atanassov, E. A. Ustinov, *ACS Appl. Mater. Interfaces* **2009**, *1*, 1623 – 1639.
[16] M. Lefevre, E. Proietti, F. Jaouen, J.-P. Dodelet, *Science* **2009**, *324*, 71 – 74.
[17] R. Bashyam, P. Zelenay, *Nature* **2006**, *443*, 63 – 66.
[18] G. Wu, K. L. More, C. M. Johnston, P. Zelenay, *Science* **2011**, *332*, 443 – 447.
[19] X. Yuan, X. Zeng, H.-J. Zhang, Z.-F. Ma, C.-Y. Wang, *J. Am. Chem. Soc.* **2010**, *132*, 1754 – 1755.
[20] W. Yang, T.-P. Fellinger, M. Antonietti, *J. Am. Chem. Soc.* **2011**, *133*, 206 – 209.
[21] *Department of Energy—Multi Year Research and Development Plan*, **2007**.
[22] K. G. Gallagher, T. F. Fuller, *Phys. Chem. Chem. Phys.* **2009**, *11*, 11557 – 11567.
[23] F. Hasché, M. Oezaslan, P. Strasser, *Phys. Chem. Chem. Phys.* **2010**, *12*, 15251 – 15258.
[24] J. Wang, G. Yin, Y. Shao, Z. Wang, Y. Gao, *J. Phys. Chem. C* **2008**, *112*, 5784 – 5789.
[25] L. Borchardt, F. Hasché, M. R. Lohe, M. Oschatz, F. Schmidt, E. Kockrick, C. Ziegler, T. Lescouet, A. Bachmatiuk, B. Büchner, D. Farrusseng, P. Strasser, S. Kaskel, *Carbon* **2012**, *50*, 1861 – 1870.
[26] B. Fang, J. H. Kim, M. Kim, M. Kim, J.-S. Yu, *Phys. Chem. Chem. Phys.* **2009**, *11*, 1380 – 1387.
[27] Y. Zhou, K. Neyerlin, T. S. Olson, S. Pylypenko, J. Bult, H. N. Dinh, T. Gennett, Z. Shao, R. O'Hayre, *Energy Environ. Sci.* **2010**, *3*, 1437 – 1446.
[28] S. Yin, S. Mu, M. Pan, Z. Fu, *J. Power Sources* **2011**, *196*, 7931 – 7936.
[29] Z.-Z. Jiang, Z.-B. Wang, Y.-Y. Chu, D.-M. Gu, G.-P. Yin, *Energy Environ. Sci.* **2011**, *4*, 2558 – 2566.
[30] Z.-Z. Jiang, Z.-B. Wang, Y.-Y. Chu, D.-M. Gu, G.-P. Yin, *Energy Environ. Sci.* **2011**, *4*, 728 – 735.
[31] K. K. R. Datta, V. V. Balasubramanian, K. Ariga, T. Mori, A. Vinu, *Chem. Eur. J.* **2011**, *17*, 3390 – 3397.
[32] N. D. Leonard, V. Nallathambi, S. C. Barton, *ECS Trans.* **2011**, *41*, 1175 – 1181.
[33] V. Nallathambi, N. Leonard, R. Kothandaraman, S. C. Barton, *Electrochem. Solid-State Lett.* **2011**, *14*, B55 – B58.
[34] J. P. Paraknowitsch, J. Zhang, D. Su, A. Thomas, M. Antonietti, *Adv. Mater.* **2010**, *22*, 87 – 92.
[35] J. P. Paraknowitsch, A. Thomas, M. Antonietti, *J. Mater. Chem.* **2010**, *20*, 6746 – 6758.
[36] F. Hasché, M. Oezaslan, P. Strasser, *ECS Trans.* **2011**, *41*, 1079 – 1088.
[37] M. Oezaslan, F. Hasché, P. Strasser, *ECS Trans.* **2010**, *33*, 333 – 341.
[38] M. Oezaslan, F. Hasché, P. Strasser, *ECS Trans.* **2011**, *41*, 1659 – 1668.
[39] *ICDD International Center for Diffraction Data*, **2002**.
[40] C. H. Hamann, A. Hamnett, W. Vielstich, *Electrochemistry*, Wiley-VCH, **2007**.
[41] A. J. Bard, M. Stratmann, *Encyclopedia of Electrochemistry*, Wiley-VCH, **2007**.
[42] N. M. Markovic, H. A. Gasteiger, B. N. Grgur, P. N. Ross, *J. Electroanal. Chem.* **1999**, *467*, 157 – 163.
[43] H. A. Gasteiger, S. S. Kocha, B. Sompalli, F. T. Wagner, *Appl. Catal. B* **2005**, *56*, 9 – 35.

[44] K. J. J. Mayrhofer, D. Strmcnik, B. B. Blizanac, V. Stamenkovic, M. Arenz, N. M. Markovic, *Electrochim. Acta* **2008**, *53*, 3181 – 3188.
[45] M. v. Laue, *Z. Kristallogr.* **1926**, *64*, 115.
[46] U. A. Paulus, T. J. Schmidt, H. A. Gasteiger, R. J. Behm, *J. Electroanal. Chem.* **2001**, *495*, 134 – 145.
[47] T. J. Schmidt, H. A. Gasteiger, G. D. Stab, P. M. Urban, D. M. Kolb, R. J. Behm, *J. Electrochem. Soc.* **1998**, *145*, 2354 – 2358.
[48] S. Koh, N. Hahn, C. Yu, P. Strasser, *J. Electrochem. Soc.* **2008**, *155*, B1281 – B1288.

Received: November 9, 2011
Revised: December 13, 2011
Published online on March 6, 2012

